A Wideband Reconfigurable Antenna with 360° Beam-Steering for 802.11ac WLAN Applications

Yang Yang, *Senior Member, IEEE,* and Xi Zhu

***Abstract*— A novel 360° beam steering patch antenna with parasitic elements is presented in this paper. The designed antenna consists of a radiating patch and six parasitic elements, each of which is connected through a group of shorting vias controlled by PIN diode switches. By switching on the desired groups of the shorting vias, the electric field distribution inside substrate cavity appears at the desired beam direction. Rotationally switching on the groups of the shorting vias, the performance of 360° beam-scanning is realized. To further understand operating mechanism, the antenna is modeled with equivalent circuit in terms of the ON and OFF status of a sector of the antenna, which can be used as a design guide for shorting-vias-controlled reconfigurable microstrip patch antennas. The fabricated antenna achieves a bandwidth of 14.5%, a peak gain of 10 dBi and the efficiency of 80.5%. The achieved beamwidths are 42° and 97° in azimuth and elevation planes, respectively. With an ability of being steered around zenith axis at six directions, the scanned beam range covers the entire 360 degrees. The physical dimension is only 2.5 λ_g for the size and 0.5 λ_g for the profile. This antenna operates from 5.1 to 5.9 GHz and has significant meaning in IEEE 802.11ac WLAN applications due to its capabilities of generating 360° steered beams.**

***Index Terms*—Beam-steering, beam-forming, WLAN, Wi-Fi, 802.11ac, high gain, reconfigurable antenna**

I. Introduction

BEAM-STEERING antennas have attracted significant attentions over the past decades due to the dramatically increasing demand for the applications of cognitive radio, cellular base station, wireless local area network (WLAN), remote sensing and satellite communications. The existing beam-steering antennas can be approximately categorized into four groups: 1) array antennas with phase control technology [1]-[5]; 2) liquid-metal antennas [6]-[7]; 3) antennas with parasitic techniques [8]-[15]; 4) circular-shaped electronically-controlled 360° beam-switching approach [16]-[24]. As an advanced function, the configuration of beam-steering antennas are normally very complicated, which causes conventional beam-steering antennas face the challenges of high profile (vertical plane), large size (horizontal plane), relatively high cost, limited bandwidth, low efficiency and limited beam-steering angle for the approaches in 1) and 3).

The above mentioned difficulties have been comprehensively studies and improved by several groups, however the challenges are still significant. In [25], [26], phase shifting techniques are specifically applied for array antennas with partially reflective surface (PRS), however the achieved beam scanning ranges are less than 60 degrees. In [27], a four-element slot antenna array was used to realize beam steering over 360° in the azimuth plane with a restricted gain around -0.5-2.1 dBi. The liquid antennas, as reported in [6], [7], brought a new horizon in beam steering technology for full range 360° scanning, but the narrow bandwidth and low gain are the disadvantages comparing with other technologies. As an important beam switching technology, the antennas with parasitic elements have been given more attentions for dynamic beam control over the past decades. This kind of antennas are usually driven by one or more radiating elements and directed by several parasitic elements at certain directions. By controlling the ON and OFF status of the switches, the parasitic elements function as directive and reflective unit forming a directional beam at certain angle [9], [13], [14], [28]. However, the reported patch antennas with parasitic elements suffer from narrow bandwidths and limited gain. Taking advantages of circular shaped geometry for patch antenna design, the capability of 360° beam scanning has been successfully realized with notable performances [19]-[24]. However, even though parasitic arrays were used in some of these designs, the reported gains were in the range of 2.1 dBi to 6.5 dBi, which could likely be further improved by introducing high order modes. Recently, some novel approaches have been proposed for 360° beam-steering technology using PIN switches [16], [17], [18]. These reported work introduced the method of 360° steering-beam by controlling the ON/OFF status of the grouped PIN diodes. However, these designs have significant drawback of large size and profile ($4.6\lambda_g$ in diameter and $1.73\lambda_g$ in profile for [16]; $1.11\lambda_g$ in diameter and $3.1\lambda_g$ in profile for [17]; $0.7\lambda_g$ in diameter and $4\lambda_g$ in profile for [18]).

Manuscript received XXX; revised XXXX; accepted XXXX. This research is supported by the Australian Research Council DE160101032.

Y. Yang and X. Zhu are with School of Electrical and Data Engineering, University of Technology Sydney, NSW 2007, Australia. (yang.yang.au@ieee.org)

Color versions of one or more of the figures in this paper are available online at http://ieeexplore.ieee.org.

Digital Object Identifier 0000

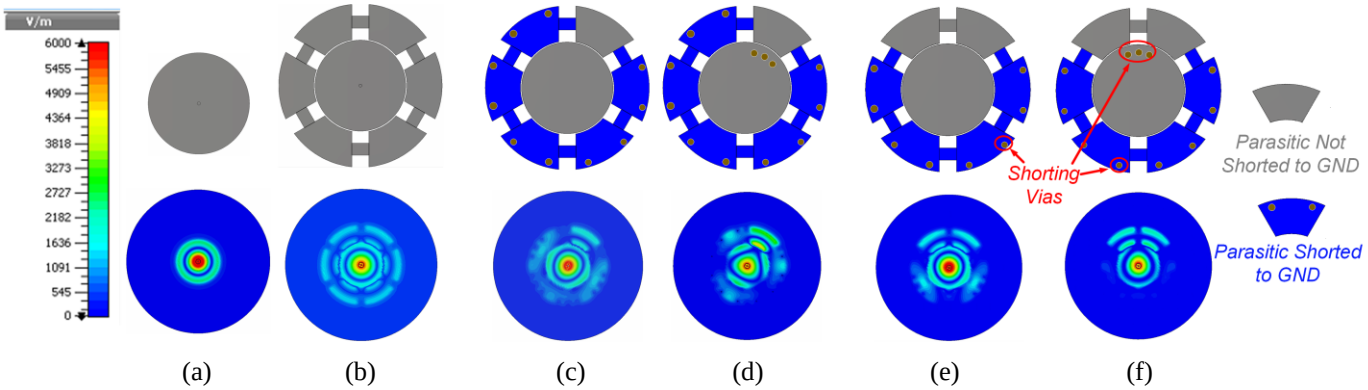

Fig. 1 Electric field distribution inside the substrate of a circular patch antenna: (a) circular patch only, (b) circular patch with stepped-ring parasitic patches, (c) one parasitic patch not shorting to the ground, without shorting vias on the center circular patch, (d) one parasitic patch not shorting to the ground, with shorting vias on the center circular patch, (e) two jointly-connected parasitic patches not shorting to the ground, without shorting vias on the center circular patch, and (f) two jointly-connected parasitic patches not shorting to the ground, with shorting vias on the center circular patch.

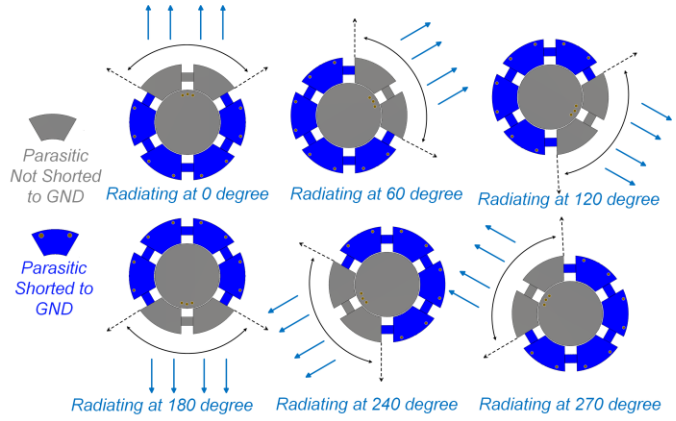

Fig. 2 Beam steering mechanism by rotationally shorting the adjacent parasitic patches to the ground.

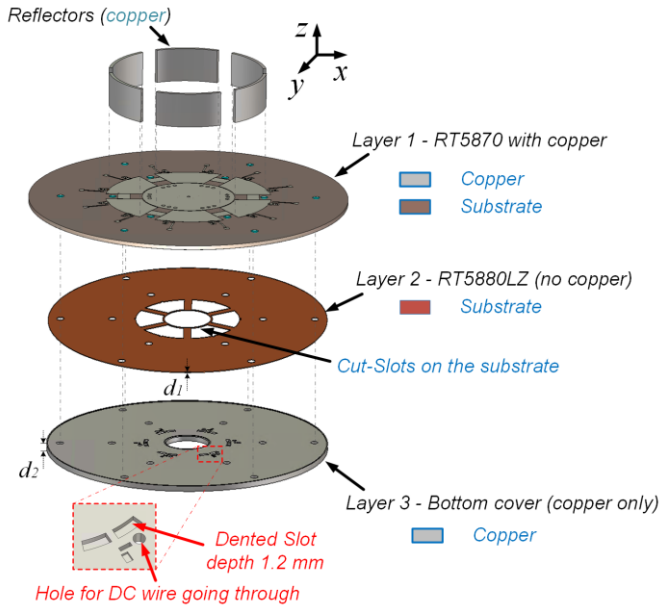

Fig. 3. Antenna configuration: oblique view of the breakdown antenna.

In this paper, a novel 360° beam scanning patch antenna with parasitic elements is proposed. The proposed design has a higher realized gain than other works using microstrip patches [22], [23] [27] and compact size compared with other high gain designs [16],[17]. By electronically controlling the status of the shorting vias on the radiating patch and parasitic patches, the electric field of the antenna can be accordingly changed appearing a strong resonance at the desired direction. The capability of 360° beam switching can be achieved over the band 5.1-5.9 GHz, which has significant meaning in IEEE standard 802.11ac for example of Wi-Fi application. The paper is organized in the following way. In Section II, the 360° beam-steering theory and antenna geometry are introduced, followed with Section III of equivalent circuit models and reconfiguration mechanism for investigation of the operational principle. Antenna performance optimization is presented Section IV. The design results and conclusions are given in Section V and Section VI, respectively.

II. Antenna Geometry

A. 360° Beam-Steering

The proposed radiating patch and parasitic patches are designed on Rogers 5870 with thickness of 1.57 mm. To verify the beam-steering concept on a patch antenna, the analysis of the electric field distribution of a circular radiating patch and surrounding parasitic patches is investigated. In Fig. 1(a), the circular patch antenna operates at TM_{02} mode with evenly distributed electric field around the center of the patch. Adding the parasitic elements jointly connected with the neighbors, as shown in Fig. 1(b), the strong resonances appear at the six directions of the circular patch, which are corresponding to the six parasitic elements. It can be seen from Fig. 1(c) that, simply applying a single sector parasitic patch and shorting the other five to the ground, the strong resonance appears at the direction that the parasitic patch is not shorted. However, there are still relatively strong electric fields at the other five directions. As is noted in Fig. 1(d), adding three shorting vias on the circular patch at the direction that the non-shorted parasitic patch applies, the non-interested electric field at the other directions tends to be weakened. To further strengthen the electric field at the desired direction while weakening the fields at other directions, two jointly-connected parasitic patches are studied as is given in Fig. 1(e) and (f). It can be seen clearly that two parasitic patches with three shorting vias on the radiating patch,

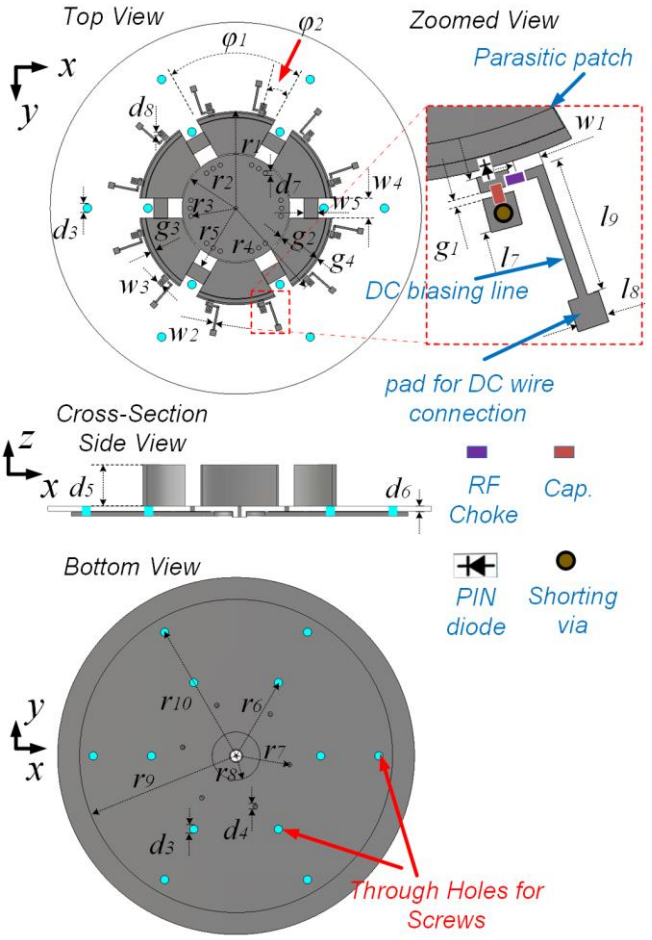

Fig. 4. Proposed antenna in top view, cross-section view and bottom view.

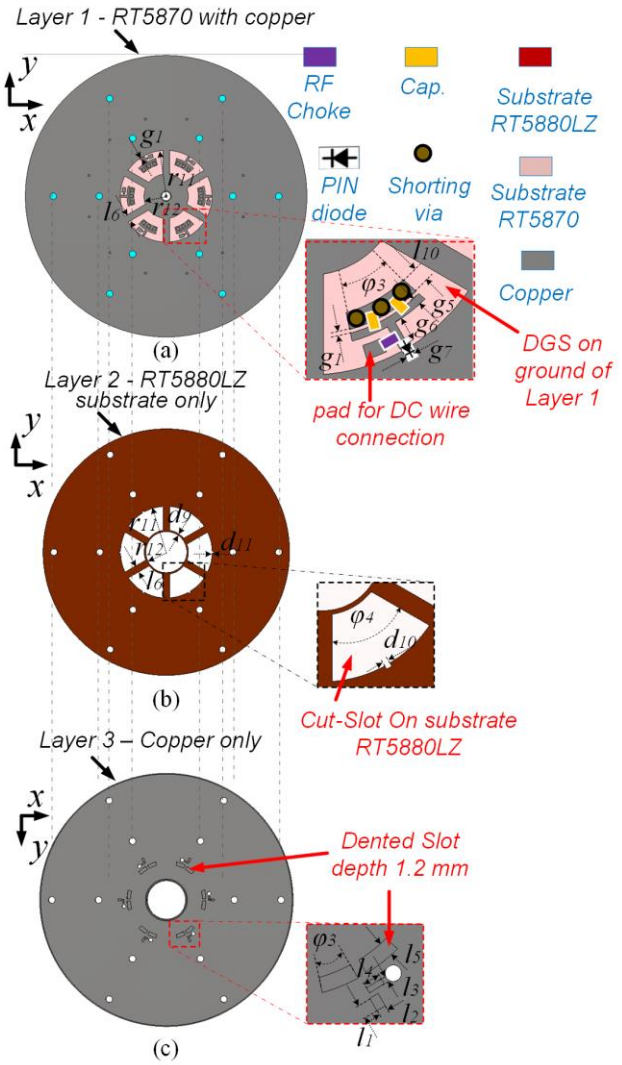

Fig. 5. Decomposed antenna: (a) bottom view of layer 1, (b) bottom view of layer 2, and (3) top view of layer 3.

configured as Fig. 1(f), can bring an excellent electric field distribution directing the radiation beam towards the desired direction. To realize the 360° planar-rotation of the electric field in Fig. 1(f), the shorting vias have to be designed with the capability of being switched-on and –off, rotationally controlling the electric field distributions of the antenna, so that the beam steering effect can be realized as shown in Fig. 2.

B. Antenna Geometry

Based on the design theory, a 360° beam-steering reconfigurable antenna is proposed using PCB substrate Rogers RT5870 (thickness 1.57 mm, ε_r = 2.33), RT5880LZ (thickness 0.254 mm, ε_r = 1.96) and metal coppers. To realize the proposed reconfiguration mechanism, PIN diodes MA4FCP300 from Macom™ are selected as the switches, which are individually used for controlling the ON- and OFF-status of each group of shorting vias.

Fig. 3 shows a breakdown diagram of the proposed antenna prototype. The antenna consists of four major sections: (1) top reflectors made by metal coppers, (2) layer 1 substrate RT5870 with coppers (copper-substrate-copper), (3) layer 2 substrate RT5880LZ (copper fully-removed), and (4) layer 3 of a bottom metal cover made by coppers. The layer 1 is the core part of the antenna, which has the radiating patch and parasitic patches as demonstrated in Fig. 3. With the copper fully removed, substrate layer 2 is used as the spacer to support layer 3. Layer 3 is made by copper and used as a shielding cover at the back side of the antenna to reduce the impact of the defected ground structures (DGS) on layer 1.

Since the shorting vias are grouped to be turned on and off for realization of beam-steering, each via group has to be isolated from the antenna patches using the specifically designed slots, where the PIN diodes are applied crossing the metal gaps (slots). According to the top view of Fig. 4, we know that the vias placed at the edge of the antenna are controlled by the PIN diodes between the parasitic patches and shorting vias on the top copper of the layer 1. This configuration can be clearly understood from the locally zoomed view in Fig. 4 that the DC power supply falls on the DC pad and the RF Choke (in purple color) blocks the RF signal from the antenna to the DC biasing line. Since all the vias connected to PIN diodes at the outer side of the parasitic patch are sharing the same ground, there is a need to have a gap between the anode side of the PIN diode and the shorting via, for the purpose of individually switching on and off the PIN diodes. The gap has to be a slot between patches and also bridged by a capacitor (in brown color) so that the RF signal

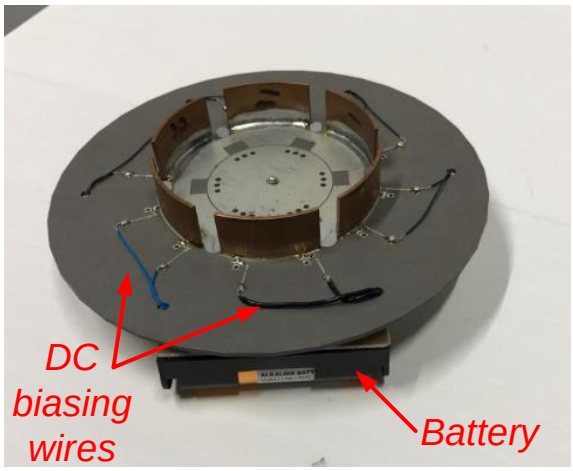

(a)

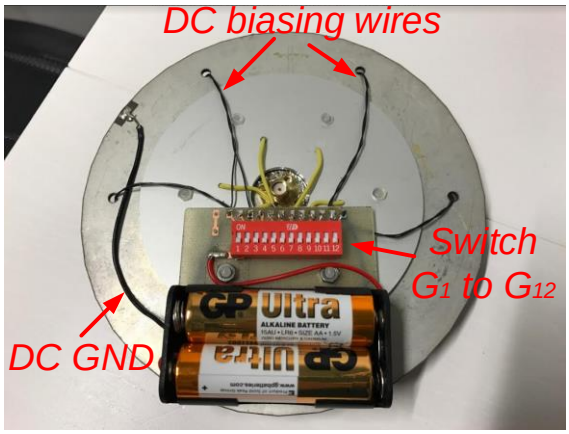

(b)

Fig. 6. Photos of the antenna prototype: (a) oblique view, (b) bottom view.

can travel from the anode side of the PIN diode to the shorting via while the DC signal is fully blocked to the ground by this bridging capacitor. The same configuration concept is also applied for the PIN diodes on the radiating patch, where the DC biasing components are mounted at the backside of the layer 1, as shown in the locally zoomed view of Fig. 5 (a).

According to Fig. 5(a), the DGS on the ground of layer 1 are applied for the purpose of individually controlling the ON- and OFF-status of the shorting vias. To effectively reduce the impact from the DGS on the ground of layer 1, layer 2 and layer 3 are employed. The layer 2 in Fig. 5(b) is used as a spacer to create a 0.25 mm air gap between the shielding layer 3 (made from metal) and the layer 1 so that the DC biasing components can be placed at the backside of the layer 1. Additionally, several dented slots are cut on the top side of the layer 3, as shown in Fig. 5(c), which are corresponding to the DC biasing components to ensure a touchless arrangement between these components and the metal cover (layer 3). The physical dimensions of this antenna are listed in Table I.

While not shown in Figs. 4 and 5, the DC wires are connected to the DC pads. For the ON status of a PIN diode, a 1.5 V DC voltage is applied on the DC pad and, consequently, the conduction between the top and bottom patches is made by the corresponding shorting via. Since the anode sides of all the PIN diodes are not physically connected (isolated by the capacitors), the DC signal is not able to flow to any of other DC

TABLE I
PHYSICAL DIMENSIONS OF THE PROPOSED ANTENNA

Sym.	VALUE	Description
ϕ_1	60°	arc radian of a parasitic sector
ϕ_2	12°	radian from outer via to the nearest parasitic side-edge
ϕ_3	60°	arc radian of a patch connected to the vias in G1-G6
ϕ_4	60°	arc radian of DGS slot on layer 2
r_1	33.8 mm	radius of the outer edge of the parasitic sector patch
r_2	18.8 mm	radius of radiating patch
r_3	16 mm	radius of the location of the shorting vias G1-G6
r_4	36.7 mm	radius of the location of the shorting vias G7-G12
r_5	23.8 mm	distance from inner edge of the joint stub to feed port
r_6	30.8 mm	radius of the location of the inner mounting screws
r_7	19.5 mm	distance of the DC wire hole to feed port
r_8	9.1 mm	radius of the inner hole on layer 3
r_9	45.2 mm	radius of the outer edge of layer 3
r_{10}	43 mm	radius of the location of the outer mounting screws
r_{11}	21.2 mm	distance from DGS outer edge to feed port
r_{12}	9.1 mm	distance from DGS inner edge to feed port
d_1	0.25 mm	thickness of layer 2
d_2	2 mm	thickness of layer 3
d_3	1.5 mm	radius of the screws
d_4	0.85 mm	radius of the holes for DC wires
d_5	14.5 mm	height of reflectors
d_6	1.57 mm	thickness of layer 1
d_7	0.8 mm	radius of the shorting vias in G1-G6
d_8	0.5 mm	radius of the shorting vias in G7-G12
d_9	0.5 mm	thickness of inner ring in layer 2
d_{10}	1 mm	slot width on layer 2 (spacing for PIN diode)
d_{11}	0.6 mm	slot depth on layer 2 (spacing for PIN diode)
w_1	1.8 mm	length of DC supply microstrip line (part 1)
w_2	0.6 mm	width of DC supply microstrip line
w_3	2 mm	pad width for shorting vias G7-G12
w_4	7 mm	distance between two adjacent parasitic patches
w_5	5 mm	width of the stub connecting adjacent parasitic patches
l_1	1.5 mm	length of the dented slot (spacing for PIN diode)
l_2	1 mm	width of the dented slot (spacing for PIN diode)
l_3	1.8 mm	length of the dented slot (spacing for RF choke)
l_4	0.6 mm	width of the dented slot (spacing for RF choke)
l_5	3 mm	width of the dented slot (spacing for cap. and vias)
l_6	3.1 mm	width of the shape between two DGS slots (layer 2)
l_7	3.9 mm	pad length for shorting vias G7-G12
l_8	2 mm	width of DC pad for G7-G12
l_9	8.6 mm	length of DC supply microstrip line (part 2)
g_1	0.3 mm	gap size for DC components
g_2	0.3 mm	gap size between radiating and parasitic patches
g_3	1.4 mm	thickness of reflector
g_4	0.7 mm	distance from reflector to parasitic outer edge
g_5	1.5 mm	width of the pad strip tapping capacitors
g_6	2.4 mm	length of pad strip tapping PIN diodes G1-G6
g_7	1 mm	width of pad strip tapping PIN diodes G1-G6

pads through the switched on shorting vias, leading to a perfect individual on-and-off control of a shorting via group. The oblique and bottom views of the fabricated antenna with batteries are shown in Fig. 6, which gives clear demonstration of the DC supply through a 1.5 V battery set.

III. ANTENNA OPERATION

A. Operation Configuration

To realize the performance in Fig. 1(f), the shorting vias are grouped as G1, G2, G3, G4, G5, G6, G7, G8, G9, G10, G11 and G12 for beam directing. Fig. 7(a) illustrates the configuration for a beam generated at 0° direction by turning on the shorting vias groups G1, G9-G12. As is shown in Fig. 7(b), the beam can be steered to 60° direction when turning on shorting vias groups

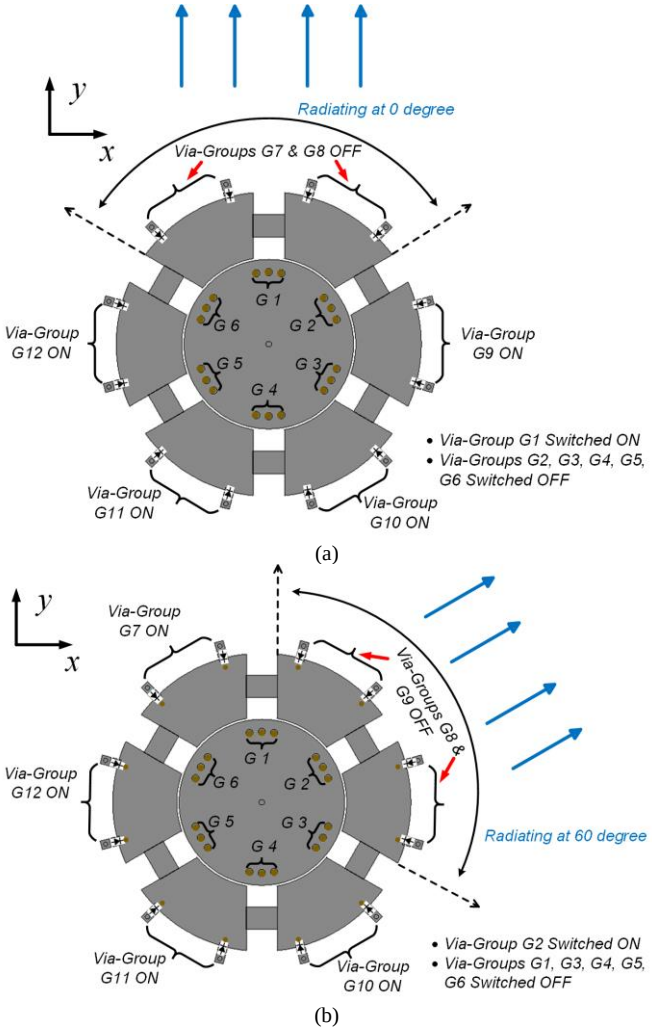

Fig. 7. Beam-steering function of the reconfigurable vias groups: (a) radiating at the direction of 0°, and (b) radiating at the direction of 60°.

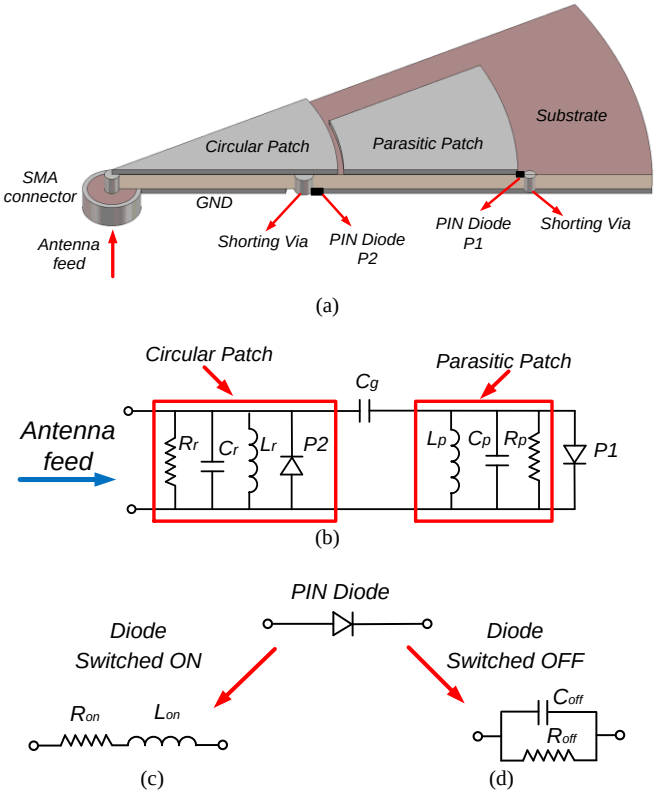

Fig. 8. One sector of the patch antenna with parasitic: (a) abstractive cut-view, (b) equivalent circuit model of a sector of the antenna, (c) circuit model of the PIN diode ON state, and (b) circuit model of the PIN diode OFF state.

TABLE II
BEAM-STEERING CONFIGURATIONS

State	Beam Direction	Via groups to be turned on	Via groups to be turned off
A	0°	G1, G9-G12	G2-G8
B	60°	G2, G7, G10-G12	G1,G3-G6,G8,G9
C	120°	G3, G7, G8, G11, G12	G1,G2,G4-G6,G9,G10
D	180°	G4, G7-G9, G12	G1-G3,G5,G6,G10,G11
E	240°	G5, G7-G10	G1-G4,G6,G11,G12
F	300°	G6, G8-G11	G1-G5,G7,G12

G2, G7, G10-G12. For the same principle, the beam can also be steered at the directions of 120°, 180°, 240° and 300°, whose configuration settings are listed in Table II.

B. Equivalent Circuit Model and Reconfiguration Mechanism

To demonstrate the switching behaviors of the resonance frequencies from a circuit point of view, the antenna is analyzed using a simplified equivalent circuit model. A sector with the cross-section view of the shorting vias is presented in Fig. 8. To demonstrate the effect of shorting vias controlled by PIN diodes, two PIN diodes are abstractively displayed in the cross-section view of the substrate, where the accurate arrangement of the shorting vias has to be referred in Figs. 4, 5 and 7.

The demonstrated sector layout and equivalent circuit models are presented in Figs. 8(a) and (b), respectively. The radiating patch and parasitic patch are modeled using *LC*-lumped components together with PIN diodes functioning as switches. According to [29], an antenna patch can be represented by a set of parallel-connected inductor, capacitor and resistor. Hence, the parasitic patch is denoted by L_p, C_p and R_p. The PIN diode P1 is connected at the edge of the parasitic patch to effectively function as a switch to short the parasitic to the ground when needed. Different to P1, PIN diode P2 controlled shorting via is placed inside the radiating patch so that the switching on and off status of the P2 cannot be simply explained as shorting the radiating patch to the ground. Instead, by switching on and off P2, it affects the local electric field intensity and can accordingly increase the resonance of the electric field when P2 is switched on and P1 is witched off (as shown in Figs. 1(c)-(f). As shown in Figs. 8(c) and (d), the ON- and OFF-status of a PIN diode can be represented by the equivalent circuit models as a series-connected *RL* circuit and a parallel-connected *RC* circuit, respectively, where the components values are R_{on} = 4 Ω, L_{on} = 0.4 nH, R_{off} = 20 kΩ and C_{off} = 0.04 pF [28].

Taking State A for example, in Fig. 9, the antenna is composed of one Equivalent Circuit A and two Equivalent Circuits B. In radiating direction, the antenna sector is represented by Equivalent Circuit A as shown in Fig. 10(a), where PIN diode P1 is switched off and P2 is switched on. On the contrary, the other two sectors at the non-radiating direction

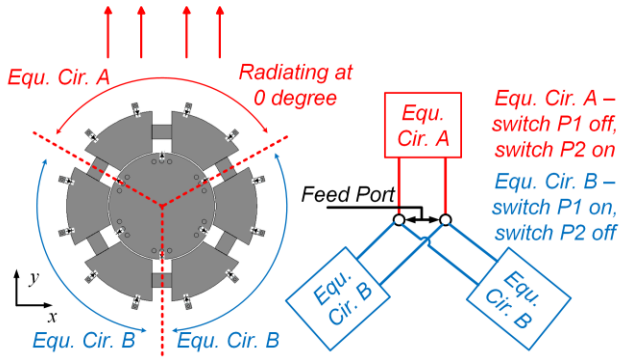

Fig. 9. Equivalent circuit of the proposed antenna functioning at State A: (a) layout view, and (b) block diagram view.

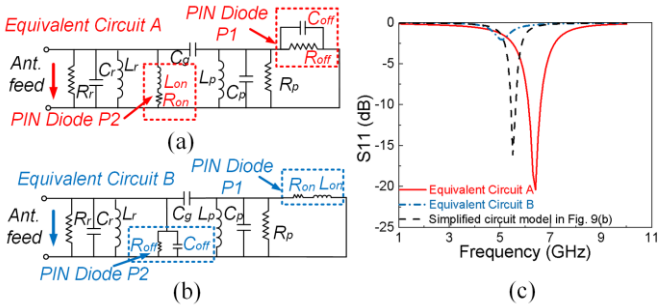

Fig. 10. Simplified circuits: (a) Equivalent Circuit A, (b) Equivalent Circuit B, and (c) reflection coefficient of Equivalent Circuits A, B and Fig. 9(b).

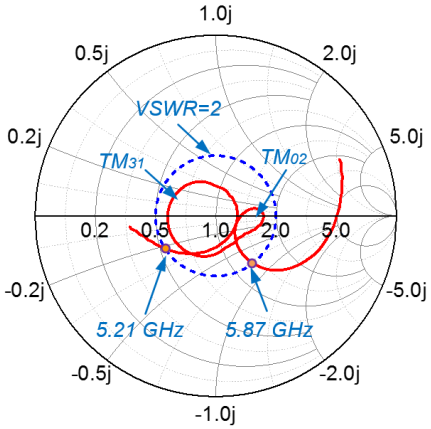

Fig. 11. Reflection coefficient on the Smith Chart.

can be represented by the circuit model presented in Fig. 10(b), where PIN diode P1 is switched on and P2 is switched off.

Fig. 10(c) shows the resonance frequencies of the Equivalent Circuits A, B and antenna equivalent circuit, respectively. In Fig. 10(c), Equivalent Circuit A indicates a resonance (S11= -21 dB) at the radiation direction, while Equivalent Circuit B appears a very weak resonance (S11= -2 dB) at the non-radiation direction, which proves the hypothesis that the electric field is significantly weakened by shorting the parasitic to the ground at the non-radiating directions. Combing one Equivalent Circuit A with two Equivalent Circuits B, the antenna circuit resonates at around 5.5 GHz with S11= -16 dB,

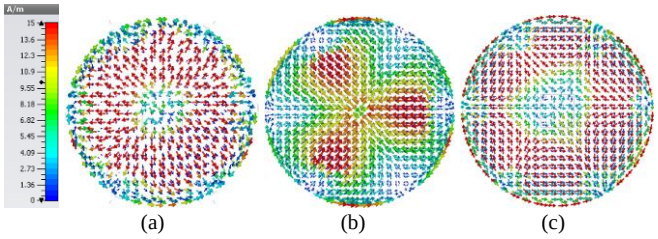

Fig. 12. Surface current distribution of the antenna resonant at: (a) TM02 mode at 5.3 GHz, (b) transition mode between TM02 and TM31 at 5.45 GHz, and (c) TM31 mode at 5.6 GHz.

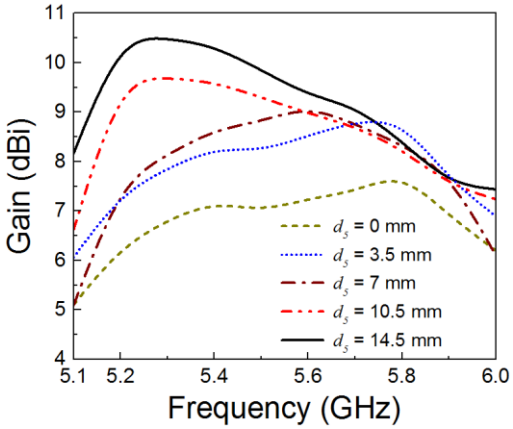

Fig. 13. Investigation on antenna gain enhancement with the varying height (d_5) of the reflectors.

indicating that the antenna equivalent circuit is dominated by Equivalent Circuit A. Therefore, the antenna is radiating towards the direction where Equivalent Circuit A applies.

The frequency responses in Fig. 10(c) are obtained from the circuit schematics in Figs. 10(a) and (b). Using schematics simulation tool ADS2016^{TM}, the following components values are obtained:

1) Antenna radiating patch: R_r = 446 Ω,C_r = 4 pF, L_r = 239.5 pH
2) Antenna parasitic patch: R_p = 120 Ω, C_p = 3 pF, L_p = 432 pH
3) Gap between radiating and parasitic patches: C_g = 0.08 pF
4) PIN diode ON status: R_{on} = 4 Ω, L_{on} = 0.4 nH
5) PIN diode OFF status: R_{off} = 20 kΩ, C_{off} = 0.04 pF

IV. Performance Optimization

A. Bandwidth Enhancement

As introduced by many other works, multi-mode operation may lead to an enhanced bandwidth [30], [31]. In this work, the radiating circular patch is specifically designed operating at TM_{02} [32]. Adding shorting vias groups G1-G6 evenly distributed at the six directions on the circular patch, the high order mode TM_{31} is generated. By tuning the distance from the vias groups G1-G6 to the feed point, the resonance frequencies of the two modes can be adjusted to form a wide bandwidth. As can be seen from Fig. 11 that two huddled circles fall in the region VSWR=2 contributing a wideband from 5.21 to 5.87 GHz. The associated surface current distributions are shown in Fig. 12. Since both TM_{02} and TM_{31} can produce conical beams, the realized dual-mode antenna is ideal for beam forming and steering by controlling the shorting vias groups as defined in Table II.

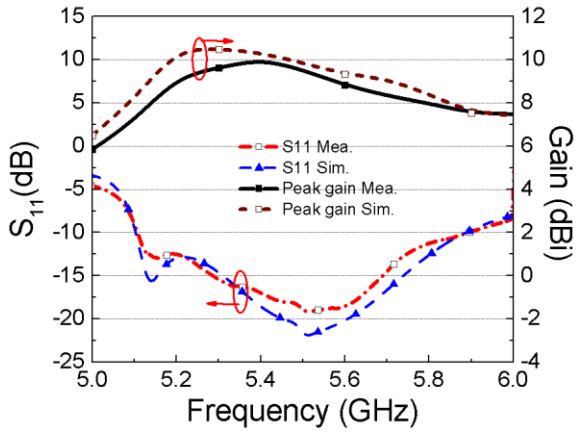

Fig. 14. Measured and simulated reflection coefficient and antenna peak gain.

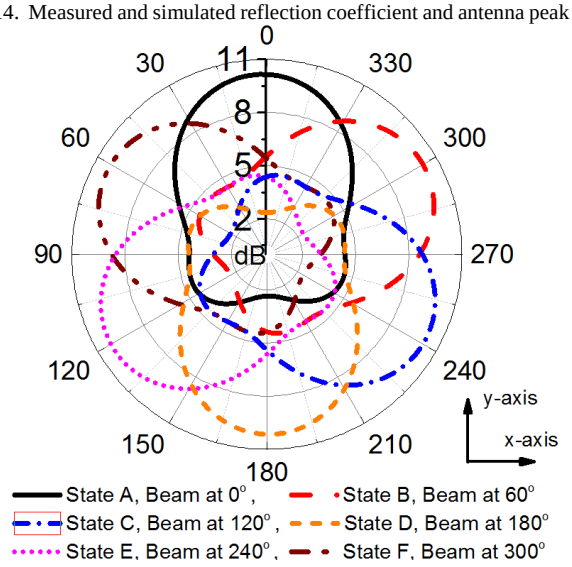

Fig. 15. Simulated beam-steering function of six different states corresponding to Table II. (Radiation pattern of the plane with constant zenith angle Theta=30° - maximum gain direction).

B. Gain Enhancement

The gain of a single microstrip patch antenna is inherently limited due to the planar arrangement of the antenna layout and relatively thin substrate ($h << \lambda_0$) [32], where h is the thickness of the substrate and λ_0 is the wavelength of the wave in free space. In this work, both parasitic patches and reflector-elements are employed and connected together, as shown in Fig. 6(a), for gain enhancement. As shown in Fig. 13, the peak gain of the antenna can be enhanced by approximately 3.2 dB when the height of the reflector d_5 is increased from 0 to 14.5 mm.

V. Simulation and Measurement Results

The full antenna prototype was designed using EM simulation tool CST 2015 and fabricated using PCB RT5870 (thickness 1.57 mm, ε_r=2.33), RT5880LZ (thickness 0.254mm, ε_r=1.96) and aluminum plates. Agilent vector network analyzer (VNA) E8361A and spherical near-field (SNF) antenna measurement system were used for the measurements of return loss and radiation patterns, respectively.

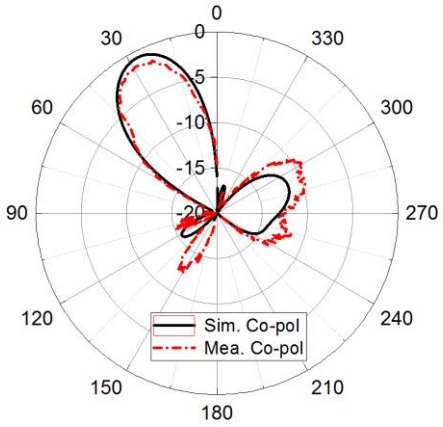

Fig. 16. Measured and simulated x-z plane radiation patterns of the proposed antenna at 5.3 GHz, State A, beam at 0° direction, (the cross-polar values are too small to be visible in the above scale).

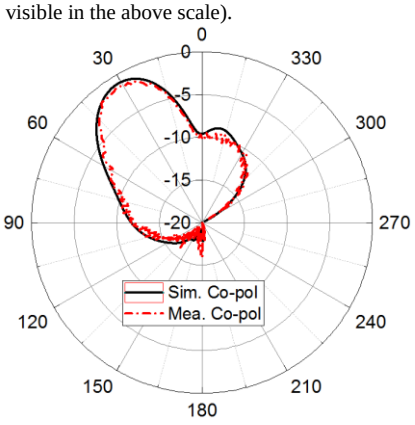

Fig. 17. Measured and simulated x-z plane radiation patterns of the proposed antenna at 5.5 GHz, State A, beam at 0° direction, (the cross-polar values are too small to be visible in the above scale).

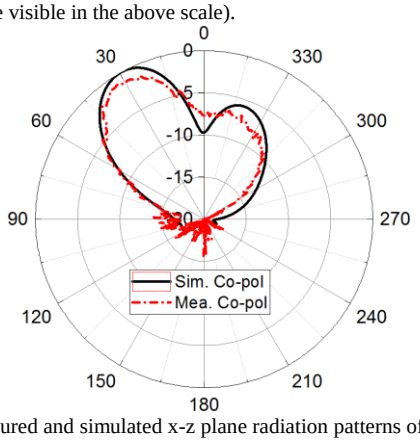

Fig. 18. Measured and simulated x-z plane radiation patterns of the proposed antenna at 5.7 GHz, State A, beam at 0° direction, (the cross-polar values are too small to be visible in the above scale).

Fig. 14 shows the simulated and measured reflection coefficients or the proposed antenna. The measured impedance bandwidth is about 14.5% for |S11| < -10 dB from 5.1 to 5.9 GHz, which is right on the spectrum scope of IEEE 802.11ac. The measured peak gain in the operation band is 10 dBi compared with the simulated one of 10.8 dBi. The difference between the measurement and simulation is likely due to the accuracy of the parasitic values of the PIN diode circuit models, assembling tolerances and connected DC cables. The measured peak value of the antenna efficiency is approximately 80.5%, which is comparable to work [16], [29].

TABLE III
COMPARISON OF THE 360° BEAM-STEERING ANTENNAS

	Size (λ_g)	Profile (λ_g)	Gain (dBi)	Bandwidth	Beamwidth	Number of the States	Reflectors /Reflective Array Used	Antenna Type	Control Method
[6]	2.04	0.01	< 0	4%	90°	N.A.	Yes	Liquid Metal	Microfluid
[12]	1.2	0.053	7.2	4%	60°	N.A.	No	Metasurface	Michanical
[16]	4.6	1.73	10	26.2%	50°	16	Yes	SIW-Horn	Electronic
[17]	1.11	3.1	7	4.5%	88°	10	Yes	AFSS	Electronic
[18]	0.7	4	13	6%	20°/70°	12	Yes	FSS array	Electronic
[19]	0.55	0.12	6.5	20%	60°	12	No	ESPAR	Electronic
[20]	0.35	0.32	4	10.3%	90°	6	No	ESPAR	Electronic
[22]	1.35	0.11	4.5	10.5%	60°	8	No	Micro. Patch	Electronic.
[23]	2.02	0.03	3.6/4.3	10.6%	67°/54°	12	No	Micro. Patch	Electronic
[27]	0.91	0.02	2.1	4%	124.5°	8/10	No	Micro. Patch	Electronic
This Work	**2.5**	**0.5**	**10**	**14.5%**	**42°/97°**	**6**	**Yes**	**Micro. Patch**	**Electronic**

Fig. 15 shows the functions of the beam-steering around zenith axis (xy-plane at constant Theta = 30°). Each beam is corresponding to a State as listed in Table II, of which the main beam directions are spaced by 60° from 0° to 360°, horizontally. The beamwidth of each of the patterns in Fig. 15 is 97° toward each direction with a sidelobe level of -4.8 dB. Thus, the 360° full-range scan can be realized by rotating the main beam direction around zenith axis (z-axis).

The simulated and measured radiation patterns at frequencies of 5.3, 5.5, and 5.7 GHz are presented in Figs. 16, 17 and 18, respectively. The patterns are plotted from x-z plane to exhibit the directivity of the beam. Due to the symmetric arrangement of the antenna configuration, only the State A is demonstrated. State B-F have nearly the same patterns as State A shows, except the main beam angle around zenith axis. According to the figures, the simulated and measured beamwidths are approximately 31° and 42°, respectively. To maintain the presentation quality of the radiation patterns, the Figs. 16-18 are scaled to -20 dB, where the cross-polarization values are too small to be visible.

VI. CONCLUSION

In this paper, a novel 360° beam steering patch antenna with parasitic elements has been presented. A three-step procedure can be summarized for designing the beam steering patch antenna using reconfigurable shorting vias. *Step 1*: achieving desired electric field distribution as shown in Fig. 1(f) for concept approval. *Step 2*: implementation of RF PIN diodes as switches for performance achievement. *Step 3*: antenna performance enhancement using external structure (in this scenario, gain enhancement by using reflectors).

This work has competitive performance with the state-of-the-art works. Even though the designs using metasurface [12] and liquid metals [6] showed relatively smaller size and profile, the bandwidth, gain and difficulties in system-integration are the inherent drawbacks of these reconfigurable mechanisms. Notably, among other works using circular patch approaches, our design achieved a high gain of 10 dBi with the capability of 360° beam-scanning around zenith axis without using the conventional approaches of horn topologies or massive arrays. The designed antenna has the excellent performance in measurement including wide bandwidth of 14.5%, high gain of 10 dBi and efficiency of 80.5%. The beamwidths are 42° and 97°, respectively, in terms of azimuth and elevation planes. Even though the proposed work has larger size compared with other designs using microstrip patches, our work successfully achieved a high gain of 10 dBi which is at least 5.5-7.9 dB higher than [22], [23], [27]. Comparing with the designs using horn, AFSS or FSS/ECCD array for high gain achievement, our design significantly reduced the size, which is only around one third of [17], one half of [18] and one seventh of [16]. This work successfully demonstrates a new concept of 360° beam steering antenna. The optimal antenna performance has been achieved for proof-of-concept at the cost of complex biasing network, which can be further simplified by optimizing the parasitic elements or improving the biasing configuration [34]. The proposed design covers the entire 5 GHz Wi-Fi band and is ideal for the IEEE 802.11ac protocol, which has been widely used in WLAN applications, such as MIMO.

ACKNOWLEDGMENT

The authors would like to thank Mr Alan Tang, Ms Mei Shen, Prof. Quan Xue, Dr. Pei-Yuan Qin for their advice and assistance with the design, experiment and fabrication. Special thanks to Roy B. V. B. Simorangkir for his time and assistance during antenna measurement.

REFERENCES

[1] C. Sun, A. Hirata, T. Ohira, and N. Karmakar, "Fast beamforming of electronically steerable parasitic array radiator antennas: Theory and experiment," *IEEE Trans. Antenna Propag*., vol. 52, no. 7, pp. 1819–1832, Jul. 2004.

[2] S. Farzaneh and A. R. Sebak, "A novel amplitude-phase weighting for analog microwave beamforming*," IEEE Trans. Antennas Propag*., vol. 54, no. 7, pp. 1997–2008, Jul. 2006

[3] D. Parker and D. C. Zimmermann, "Phased arrays-Part 1: theory and architectures," *IEEE Trans. Microw. Theory Tech.*, vol. 50, no. 3, pp. 678– 687, Mar. 2002.

[4] E. Topak, J. Hasch, C. Wagner, and T. Zwick, "A novel millimeter-wave dual-fed phased array for beam steering," *IEEE Trans. Microw. Theory Tech*., vol. 61, no. 8, pp. 3140–3147, Aug. 2013.

[5] R. Guzmán-Quirós, A. R. Weily, J. L. Gómez-Tornero and Y. J. Guo, "A Fabry–Pérot antenna with two-dimensional electronic beam scanning," *IEEE Trans. Antennas Propag*., vol. 64, no. 4, pp. 1536-1541, Apr. 2016.

[6] D. Rodrigo, L. Jofre, and B. A. Cetiner, "Circular beam-steering reconfigurable antenna with liquid metal parasitics," *IEEE Trans. Antennas Propag.*, vol. 60, no. 4, pp. 1796–1802, Apr. 2012.
[7] A. A. Gheethan, M. C. Jo, R. Guldiken and G. Mumcu, "Microfluidic based Ka-band beam-scanning focal plane array*," IEEE Antennas and Wirel. Propag. Letts.*, Vol. 12, pp. 1638-1641, Dec. 2013.
[8] S. V. S. Nair and M. J. Ammann, "Reconfigurable antenna with elevation and azimuth beam switching," *IEEE Antennas and Wirel. Propag. Letts.*, Vol. 9, pp. 367-370, May, 2010.
[9] Z. Li, E. Ahmed, A. M. Eltawil, and B. A. Cetiner, "A beam-steering reconfigurable antenna for WLAN applications," *IEEE Trans. Antennas Propag.*, vol. 63, no. 1, pp. 24–32, Jan. 2015.
[10] Z. Li, H. Mopidevi, O. Kaynar and B. A. Cetiner, "Beam-steering antenna based on parasitic layer," *Electronics. Lett*., Vol. 48, no. 2, pp. 59-60, Jan. 2012.
[11] L. Akhoondzadeh-Asl, J. J. Laurin, and A. Mirkamali, "A novel low-profile monopole antenna with beam switching capabilities*," IEEE Trans. Antennas Propag.*, vol. 62, no. 3, pp. 1212-1220, Mar. 2014.
[12] H. Zhu, S. Cheung, and T. Yuk, "Mechanically pattern reconfigurable antenna using metasurface," *IET Microw., Antennas Propag.*, vol. 9, no. 12, pp. 1331–1336, Sep. 17, 2015.
[13] M. Jusoh, T. Aboufoul, T. Sabapathy, A. Alomainy and M. R. Kamarudin, "Pattern-reconfigurable microstrip patch antenna with multidirectional beam for WiMAX application," *IEEE Trans. Antennas Propag*., vol. 13, pp. 860-863, Apr. 2014.
[14] S. J. Shi and W. P. Ding, "Radiation pattern reconfigurable microstrip antenna for WiMAX application," *Electronics Lett.*, vol. 51, no. 9, pp. 662-664, Apr. 2015.
[15] M. S. Alam and A. Abbosh, "Wideband pattern-reconfigurable antenna using pair of radial radiators on truncated ground with switchable director and reflector," *IEEE Antennas and Wirel. Propag. Letts.*, vol. 16, pp. 24-28, 2017.
[16] L. Ge, K. M. Luk and S. Chen, "360-degree beam-steering reconfigurable wideband substrate integrated waveguide horn antenna," *IEEE Trans. Antennas Propag.*, vol. 64, no. 12, pp. 5005–5011, Oct. 2016.
[17] L. Zhang, Q. Wu and T. A. Denidni, "Electronically radiation pattern steerable antennas using active frequency selective surfaces," *IEEE Trans. Antennas Propag.*, vol. 61, no. 12, pp. 6000-6007, Dec. 2013.
[18] A. Edalati and T. A. Denidni, "High-gain reconfigurable sectorial antenna using an active cylindrical FSS structure," *IEEE Trans. Antennas Propag*., vol. 59, no. 7, pp. 2464–2472, Jul. 2011.
[19] H., Liu, S. Gao and T. H. Loh, "Compact dual-band antenna with electronic beam-steering and beamforming capability," *IEEE Antennas and Wirel. Propag. Letts.*, vol. 10, pp. 1349-1352, Nov. 2011.
[20] L. Hai-Tao, S. Gao and L. Tian-Hong, "Electrically small and low cost smart antenna for wireless communication," *IEEE Trans. Antennas Propag.*, vol. 60, no. 3, pp. 1540–1549, Mar. 2012.
[21] N. Nguyen-Trong, A. Piotrowski, L. Hall and C. Fumeaux, "A frequency- and polarization-reconfigurable circular cavity antenna," *IEEE Antennas and Wirel. Propag. Letts.*, vol. 16, pp. 999-1002, 2017.
[22] M. S. Alam and A. Abbosh, "Planar pattern reconfigurable antenna with eight switchable beams for WiMax and WLAN applications," *IET Microw., Antennas Propag.*, vol. 10, no. 10, pp. 1030-1035, Jul. 2016.
[23] T. Guo, W. Leng, A. Wang, J. Li and Q. Zhang, "A novel planar parasitic array antenna with frequency- and pattern-reconfigurable characteristics," *IEEE Antennas Wirel. Propag. Lett*., vol. 13, pp. 1569–1572, Aug. 2014.
[24] M. S. Alam and A. Abbosh, "Beam-steerable planar antenna using circular disc and four PIN-controlled tapered stubs for WiMAX and WLAN applications," *IEEE Antennas Wirel. Propag. Lett*., vol. 15, pp. 980–983, 2016.
[25] T. Debogovic and J. Perruisseau-Carrier, "Array-fed partially reflective surface antenna with independent scanning and beamwidth dynamic control," *IEEE Trans. Antenna Propag.*, vol. 62, no. 1, pp. 446–449, Jan. 2014.
[26] L. Ji, G. Fu and S.-X. Gong, "Array-fed beam-scanning partially reflective surface (PRS) antenna," *Progress in Electromagnetics Res. Lett.* Vol. 58, pp. 73-79, 2016.
[27] M.-I. Lai, T.-Y. Wu, J.-C. Wang, C.-H. Wang, and S. Jeng, "Compact switched-beam antenna employing a four-element slot antenna array for digital home applications," *IEEE Trans. Antennas Propag*., vol. 56, no. 9, pp. 2929–2936, Sep. 2008.
[28] P. Y. Qin, Y. J. Guo, and C. Ding, "A beam switching quasi-yagi dipole antenna," *IEEE Trans. Antennas Propag.*, vol. 61, no. 10, pp. 4891–4899, Oct. 2013.
[29] L. Ge and K.-M. Luk, "Frequency-reconfigurable low-profile circular monopolar patch antenna," *IEEE Trans. Antennas Propag.*, vol. 62, no. 7, pp. 3443–3449, Jul. 2014.
[30] N.-W. Liu, L. Zhu, W.-W. Choi and X. Zhang, "A low-profile aperture-coupled microstrip antenna with enhanced bandwidth under dual-resonance," *IEEE Trans. Antennas Propag.*, early access, DOI: 10.1109/TAP.2017.2657486.
[31] J. Liu, Q. Xue, H. Wong, H. W. Lai and Y. Long, "Design and analysis of a low-profile and broadband microstrip monopolar patch antenna," *IEEE Trans. Antennas Propag.*, vol. 61, no. 1, pp. 11–18, Jan. 2013.
[32] R. Garg, P. Bhartia, I. Bahl and A. Ittipiboon, "Microstrip antenna design handbook," Artech House, Boston, 2000, pp. 317–398.
[33] CST Studio Suit 2015. Computer Simulation Technology, Darmstadt, Germany.
[34] Y. Yang, R. B. V. B. Simorangkir, X. Zhu, K. Esselle and Q. Xue, "A novel boresight and conical pattern reconfigurable antenna with the diversity of 360° polarization scanning," *IEEE Trans. Antennas Propag.*, vol. 65, no. 11, pp. 5747–5756, Nov. 2017.

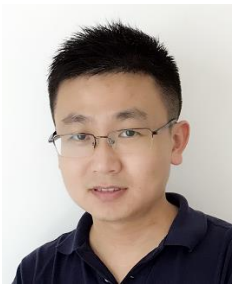

Yang Yang (S'11–M'14-SM'17) was born in Bayan Nur, Inner Mongolia, China and received the PhD degree from Monash University, Melbourne, Australia, in 2013. From July 2012 to April 2015, he was an Asia Pacific GSP Engineer at Rain Bird and a Global GSP Success Award holder of the year 2014. From April 2015 to April 2016, he served as a Senior Research Associate with Department of Engineering, Macquarie University, Sydney, Australia.

From April 2016 to December 2016, he was a Research Fellow with State Key Laboratory of Millimeter-Waves, City University of Hong Kong. In the same year, he has been involved in National Basic Research Program of China (973 Program) and appointed as an honorary research fellow with Shenzhen Institute, City University of Hong Kong. In December 2016, Dr. Yang joined University of Technology Sydney, Australia, as a lecturer. His research interests include RFIC, microwave and millimeter-wave circuits and systems, reconfigurable antennas, wearable antennas and wearable medical sensing devices and systems.

Xi Zhu received the B.E. (Hons.) and PhD from University of Hertfordshire (UH), Hertfordshire, UK, in 2005 and 2008, respectively. He is currently a Lecturer with the School of Computing and Communication, University of Technology Sydney, NSW, Australia. His research activities mainly involve in the areas of analogue baseband, radio frequency (RF) and mm-wave circuits and systems designs. He has co-authored over 60 refereed publications in the above-mentioned fields.